# Parametric Study on the S-Bosch Process via a Comprehensive Mathematical Model

Jesus A. Dominguez
*Insight Global/Amentum's Space Exploration Division (ASED), Huntsville, AL, 35806*

Timothy Giesy
*TRISO-X, Oak Ridge, TN, 37830*

Jeff Mehan, Kathryn Ollenburg
*Amentum's Space Exploration Division (ASED), Huntsville, AL, 35806*

**One crucial task of Environmental Control and Life Support Systems (ECLSS) is to efficiently recover closed-loop oxygen ($O_2$) from metabolic carbon dioxide ($CO_2$) to revitalize the breathing air. The current state-of-the-art (SOA) for the International Space Station (ISS) uses a Sabatier reaction in a system with a 50% $O_2$ recovery rate. The Series-Bosch (S-Bosch) is an alternative NASA is considering as, unlike the Sabatier, which has theoretical limits on maximum $O_2$ recovery, the S-Bosch process can theoretically recover all the $O_2$ from metabolic $CO_2$ with only solid carbon (C) as a byproduct. A comprehensive mathematical model of a tubular S-Bosch reactor has been implemented to conduct a kinetics study on all three coupled S-Bosch reactions: reverse water-gas shift (RWGS), hydrogenation, and Boudouard. The model includes general mass balance, species mass balance, momentum balance, energy balance, solid carbon-graphite mass generation through the reactor, volumetric void reduction due to solid carbon-graphite deposition, Darcy permeability variation due to solid carbon-graphite deposition, equilibrium reactions, reaction kinetics rate, and catalyst degradation due to solid-graphite deposition. The temperature-dependent equilibrium and kinetics reaction rate expressions are taken from the literature, they will be experimentally determined in-house via a kinetics study in the future to validate the S-Bosch reactor model, allowing the implementation of a parametric study and optimization of the S-Bosch process with a high degree of confidence. Using the equilibrium and kinetics reaction rate parameters published in the literature we present a preliminary parametric study and further optimization to qualitatively estimate the inlet process conditions, such as gas temperature, gas pressure, $CO_2/H_2$ composition ratio, and inlet gas velocity that optimize, via the Levenberg–Marquardt algorithm (LMA), the reduction of $CO_2$ to solid carbon.**

## Nomenclature

| | | |
|---|---|---|
| AR | = | Atmospheric revitalization |
| C | = | Carbon |
| $CO_2$ | = | Carbon dioxide |
| CO | = | Carbon monoxide |
| ECLSS | = | Environmental Control and Life Support System |
| LMA | = | Levenberg–Marquardt algorithm |
| $H_2$ | = | Hydrogen |
| $H_2O$ | = | Water |
| MMA | = | Method of Moving Asymptotes |
| MSFC | = | Marshall Space Flight Center |
| NASA | = | National Aeronautics and Space Administration |
| ISS | = | International Space Station |
| PDE | = | Partial differential equations |
| RWGS | = | Reverse water-gas shift |
| S-Bosch | = | Series-Bosch |
| SOA | = | State of the art |
| SNOPT | = | Sparse Nonlinear OPTimizer |
| SS | = | Stainless steel |

# I. Introduction

One crucial task of Environmental Control and Life Support Systems (ECLSS) is to efficiently recover closed-loop oxygen ($O_2$) from metabolic carbon dioxide ($CO_2$) to revitalize the breathing air. The current state-of-the-art (SOA) for the International Space Station (ISS) uses a Sabatier reaction in a system with a 50% O2 recovery rate. The Series-Bosch (S-Bosch) is an alternative NASA is considering as, unlike the Sabatier, which has theoretical limits on maximum $O_2$ recovery, the S-Bosch process can theoretically recover all the $O_2$ from metabolic $CO_2$ with only solid carbon-graphite as a byproduct. The S-Bosch process involves reacting $CO_2$ and $H_2$ to produce solid carbon and $H_2O$ via three coupled reactions: the reverse water-gas shift (RWGS), hydrogenation, and Boudouard reactions. The resultant products of all three reactions are solid carbon and $H_2O$ from $CO_2$ and $H_2$. The three S-Bosch reactions and the single resultant reaction are shown below.

| | | |
|---|---|---|
| $CO_2 + H_2 \leftrightarrows CO + H_2O$ | Reverse water-shift (RWGS) reaction | (1) |
| $CO + H2 \leftrightarrows C(s) + H_2O$ | Hydrogenation reaction | (2) |
| $2CO \leftrightarrows C(s) + CO_2$ | Boudouard reaction | (3) |
| $CO_2 + 2H_2 \leftrightarrows C(s) + 2H_2O$ | Overall reaction | (4) |

The S-Bosch reaction requires high temperatures (650-850 °C) to achieve high $CO_2$ conversion and mitigate the formation of methane ($CH_4$) due to Sabatier side reactions (Equations 5 and 6), which consume necessary reactants at temperatures below 650 °C, as demonstrated by Saurabh et al.,[1], among others.

| | | |
|---|---|---|
| $CO_2 + 4H_2 \rightarrow CH_4 + 2H_2O$ | Sabatier side-reaction | (5) |
| $CO + 3H_2 \rightarrow CH_4 + H_2O$ | Sabatier side-reaction | (6) |

The S-Bosch reactions are activated in the presence of a catalyst (e.g., iron, cobalt, nickel, or ruthenium) housed in a packed bed reactor with high porosity. In a typical reactor, the gas enters the core of a tubular packed reactor, and a set of external heating rods provide controlled heat flux to reach the desired operating temperature.

A comprehensive and rigorous mathematical model of a packed-bed reactor has been implemented to conduct 1) kinetics studies on different catalysts for all three coupled S-Bosch reactions (reverse water-gas shift (RWGS), hydrogenation, and Boudouard) and 2) S-Bosch process optimization to determine the process conditions that maximize the $CO_2$ conversion to $O_2$ and solid carbon.

Using the equilibrium and kinetics reaction rate parameters published in the literature we present a preliminary parametric study and further optimization to qualitatively estimate the inlet process conditions, such as gas temperature, gas pressure, $CO_2/H_2$ composition ratio, and inlet gas velocity that optimize, via the Levenberg–Marquardt algorithm (LMA), the reduction of $CO_2$ to solid carbon.

# II. Model Formulation

## A. Mathematical Approach

The model is represented via a set of partial differential equations (PDE) that describe the different coupled physics processes (multiphysics) that occur in an annular reactor packed with catalysis beans, forming a porous medium in which the gas phase is in contact with the catalysis surface. The PDE-based model, solved using COMSOL multiphysics software, also considers that the $CO_2$ gaseous phase changes to a solid phase (carbon-graphite) and is deposited on the catalysis surface, degrading the catalysis availability, the voided volumetric space of the reactor, and the porosity permeability in the reactor. The multiphysics processes included in the model are:

1) General mass balance
2) Species mass balance
3) Momentum balance
4) Energy balance
5) Solid carbon-graphite mass generation through the reactor
6) Volumetric void reduction due to solid carbon-graphite deposition
7) Darcy permeability variation due to solid carbon-graphite deposition
8) Equilibria reaction constants
9) Reaction kinetics rate
10) Catalysis degradation due to solid-graphite deposition

***General mass balance***: The continuity equation 7 accounts for the general mass balance in any non-nuclear continuum mechanics analysis. The equation is developed by adding up the rate at which mass flows in and out of a control volume and setting the net in-flow equal to the rate of change of mass within it.

$$\frac{\partial}{\partial t}\left(\varepsilon_p \rho\right) + \nabla.(\rho u) = Q_m \tag{7}$$

Where

$u$ Gas velocity vector (m/s)
$\rho$ Gas density (kg/m$^3$)
$\varepsilon_p$ porosity of porous medium (-)
$Q_m$ mass source or sink (kg/(m$^3$.s))

The mass generated and consumed due to S-Bosch reactions is included in Equation 7 through the mass or sink term ($Q_m$). The density $\rho$ varies and depends on the pressure, temperature, and composition according to the ideal gas law.

***2) Specie mass balance***: A species mass balance Equations 8 and 9 track the species in a control volume, neglecting the migration of the species in an electric field.

$$\frac{\partial}{\partial t}(\rho C_i) + \nabla.(\rho C_i \hat{u}) = \nabla.(D_{im} \nabla C_i) + R_i \tag{8}$$

$$j_i = -D_{im} \nabla C_i \tag{9}$$

Where

$C_i$ Molar concentration of species i (mol/m$^3$)
$R_i$ Reaction rate expression for species i (mol/(m$^3$.s))
$\hat{u}$ Mass average velocity vector (m/s)
$j_i$ Mass flux diffusive flux vector for specie i (mol/(m$^2$.s)
$D_{im}$ Diffusion coefficient of species i within the gas mixture (m$^2$/s)

The diffusion coefficient of a species i within the gas mixture $D_{im}$ is estimated using the Maxwell–Stefan approach, which employs the most detailed diffusion model and requires that all component pairs' multicomponent Maxwell–Stefan diffusivities are known.

***3) Momentum balance***: The Brinkman Equation 10 calculates fluid velocity and pressure fields of single-phase flow in porous media in the laminar flow regime. The physics interface extends Darcy's law to describe the kinetic energy dissipation by viscous shear, similar to the Navier–Stokes equations. The influence of gravity and other volume forces is accounted for via the force term F (kg/(m$^2$·s$^2$)).

$$\frac{\rho}{\varepsilon_p}\left(\frac{\partial u}{\partial t} + (u.\nabla)\frac{u}{\varepsilon_p}\right) = -\nabla \mathrm{p} + \nabla.\left[\frac{1}{\varepsilon_p}\left\{\mu(\nabla \mathrm{u} + (\nabla \mathrm{u})^T) - \frac{2}{3}\mu(\nabla \mathrm{u})I\right\}\right] - \left[k^{-1}\mu + \frac{Q_m}{{\varepsilon_p}^2}\right]u + F \tag{10}$$

Where

μ Viscosity (kg/(m.s)
$k$ Darcy permeability of porous medium (m$^2$)
$I$ Identity matrix.
$F$ External force (kg/(m$^2$·s$^2$))

***4) Energy balance:*** The influence of the temperature on the equilibrium reaction and reaction rate is significant. The reaction rate increases as the fluid flows through the reactor and is heated by the walls and the heat of the reaction. The energy balance is illustrated in Equation 5.

$$\rho C_p \frac{\partial T}{\partial t} + \nabla.(-K\nabla T) = \sum_i \vartheta_{i,j} H_j r_i + h_r A_r (T_w - T) - \rho C_p (u.\nabla T) + Q \tag{11}$$

Where

T Gas temperature (K)
$T_w$ Reactor wall temperature (K)
$r_i$ Reaction rate of reaction i (mol/m$^3$-hr)
$\vartheta_{i,j}$ Reaction coefficient of component j in the reaction i (-)
$h_r$ Convective heat transfer coefficient
$A_r$ Specific area of the catalyst particles (m$^2$)
$K$ Thermal conductivity (W/(m.K))

$C_p$ Specific heat capacity (J/(kg·K))
$H_j$ Enthalpy of component j in the reaction i (KJoule/mol)
$Q$ External heat source (W/m)

The third term of Equation 11) is the heat of the reaction that is temperature-dependent, while the fourth term is associated with heat loss to the reactor wall. Convective and diffusion heat transfer contributions are not neglected in the model; the second and fifth terms in Equation 11) correspond to the diffusion and convective heat transfer contributions, respectively.

***5) Solid carbon-graphite mass generation through the reactor:*** The carbon generated in the hydrogenation and Boudouard reactions (equations 2 and 3 respectively) turns into a solid phase. The total solid carbon formed and deposited on the catalysis surface is determined by integrating the carbon generated through the reactor volume as established in Equation 6.

$$m_s = \frac{M_i}{V} \int C_i dV \tag{12}$$

Where
$m_s$ Solid carbon within the reactor
$M_i$ Carbon molecular weight
$C_i$ Carbon concentration generated in reactions of equations 2 and 3.

***6) Volumetric void reduction due to solid carbon-graphite deposition:*** The reactor's volumetric void fraction, εp, changes with solid carbon formation, as established in Equation 13.

$$\frac{\partial \varepsilon_p}{\partial t} = \frac{1}{\rho_i} \frac{\partial C_i}{\partial t} \tag{13}$$

Where
$\rho_i$ Carbon density (2,250 kg/m$^3$)

According to Darcy's law, the expression in Equation 7 influences the pressure-flow characteristics of the reactor.

***7) Darcy permeability variation due to solid carbon-graphite deposition:*** The Darcy permeability k is a function of void fraction εp$^2$. This dependency has been regressed in other studies.[3] The Darcy permeability is a function of total reactor solid carbon mass ms obtained from Equation 14.

$$\log(k) = -9.2876 \quad \text{for ms} < 360.6 \text{ kg/m3}$$
$$\log(k) = -0.001854ms - 8.6190 \quad \text{for ms} \geqq 360.6 \text{ kg/m3} \tag{14}$$

***8) Equilibrium reaction constants:*** The RWGS, hydrogenation, and Boudouard reactions (Equations 1, 2, and 3) are all equilibrium processes. Therefore, the relative deviation in composition from equilibrium determines how much the reaction will occur and affects the reaction kinetics, which are concentration-temperature dependent. For the general reaction equation, an equilibrium constant can be expressed as:

$$\alpha A + \beta B \leftrightarrows \gamma C + \delta D \tag{15}$$

$$\kappa = \prod_j X_j^{\vartheta_j} = \frac{[a_C]^{\gamma}[a_D]^{\delta}}{[a_A]^{\alpha}[a_B]^{\beta}} \tag{16}$$

Where
$\kappa$ Equilibrium constant
$\alpha, \beta, \gamma, \delta$ Reaction coefficients of components *A, B, C,* and *D*, respectively.
$a_A$ Activity coefficient of component *A*
$a_B$ Activity coefficient of component *B*
$a_C$ Activity coefficient of component *C*
$a_D$ Activity coefficient of component *D*

Rigorous method to calculate the equilibrium activity coefficients and the respective equilibrium constant can be found in Sandler's work[4]. The temperature-dependent equilibrium constants used in the model for all three reactions are empirically determined and have a general form:

$$\kappa = exp\left[\frac{\lambda_1}{T^2} + \frac{\lambda_2}{T} + \lambda_3\right] \quad (17)$$

Where

$\kappa$ Equilibrium constant (-)
T Temperature (K)
$\lambda_1$ , $\lambda_2$ , $\lambda_3$ Constants

Equation 17 is much easier to implement numerically than Equation 16 via Sandler's approach[4], and both the rigorous (Equation 16) and the empirical (Equation 17) derivations show good agreement. Table 1 lists the parameter values $\lambda_1$, $\lambda_2$, and $\lambda_3$ for the three reactions (Equations 1, 2, and 3, respectively). Figure 1 shows the log values of these three equilibrium constants within a temperature range of 500-900 °C.

**Table 1. Parameters values of equilibrium constant (Equation 17) for the three Bosch-S reactions.**

| | Reaction | | $\lambda_1$ | $\lambda_2$ | $\lambda_3$ |
|---|---|---|---|---|---|
| 1 | RWGS | $CO_2 + H_2 \leftrightarrows CO + H_2O$ | -191,928.1 | -3,937.4 | 3.8143 |
| 2 | Hydrogenation | $CO + H_2 \leftrightarrows C(s) + H_2O$ | -121,003.4 | 16,573.0 | -17.3858 |
| 3 | Boudouard | $2CO \leftrightarrows C(s) + CO_2$ | 70,924.7 | 20,510.4 | -21.2000 |

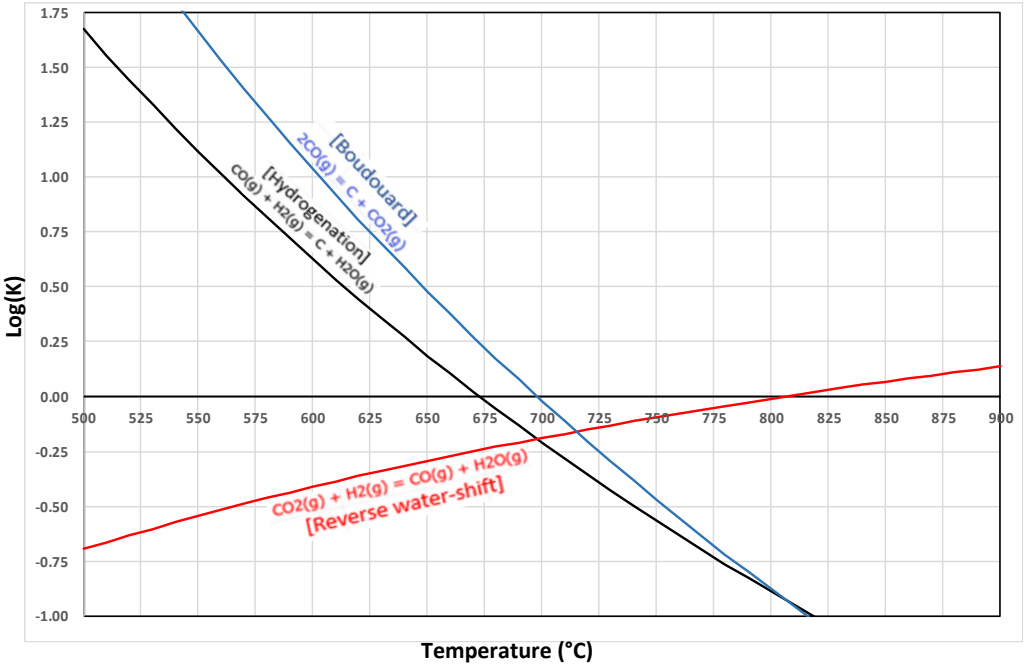


**Fig. 1. Equilibrium Constant for RWGS, Hydrogeneration, and Boudouard reactions using the parameters listed in Table 1.**

Log equilibrium constants for RWGS, hydrogenation, and Boudouard reactions are zero at 810, 675, and 700 °C, respectively, showing that above these temperature values, the equilibrium turns to favor the product side of the equilibrium reaction. Hydrogenation and Boudouard equilibrium favor the reactants, and their constant values get closer as temperature increases, reaching zero values at 675 and 700 °C, respectively. In contrast, the RWGS equilibrium favors the product at low temperatures and reaches zero value at 800 °C.

***9) Kinetics reaction rates:*** The kinetics reaction rate through which each reaction occurs depends upon the composition of the reactants, the reactor pressure, the catalyst material, the reaction temperature, and the carbonization effect in hydrogenation and Boudouard reactions. The formulation of the gas-phase equilibria reaction kinetics for reactions 1 (RWGS) and 2 (hydrogenation) follows the approach published by Fritts[5] and is summarized below.

$$r_1 = \tau_1 \rho P\left(x_{CO_2} x_{H_2} \kappa_1 - x_{CO} x_{H_2O}\right) \quad \text{[RWGS reaction, Equation 1]} \quad (18)$$

$$r_2 = \tau_2 \rho P\left(x_{CO} x_{H_2} \kappa_2 - x_{H_2O}\right) \quad \text{[Hydrogenation reaction, Equation 2]} \quad (19)$$

$$\tau_1 = \tau_{r,1} exp\left(\frac{\Delta h_{r,1}}{R_g T}\right) \quad (20)$$

$$\tau_2 = \tau_{r,2} exp\left(\frac{\Delta h_{r,2}}{R_g T}\right) \quad (21)$$

Where
$r_1$ RWGS reaction rate (mol/m$^3$-hr)
$r_2$ Hydrogenation reaction rate (mol/m$^3$-hr)
$\tau_1$ RWGS reaction rate coefficient (1/(bar-hr))
$\tau_2$ Hydrogenation reaction rate coefficient (1/(bar-hr))
$x_i$ Mole fraction of component i = 1, 2, 3 (-)
$\tau_{r,1}$ Reference RWGS reaction rate coefficient (1/(bar-hr)
$\tau_{r,2}$ Reference hydrogenation reaction rate coefficient (1/(bar-hr))
$\Delta h_{r,1}$ Reference RWGS activation energy (Joule/mole)
$\Delta h_{r,2}$ Reference hydrogenation activation energy (Joule/mole)

**Table 2. Kinetics rate coefficients (Equations 21, 22 and 23) for the three Bosch-S reactions**

| i | Reaction | | $\tau_{r,i}$ (bar/hr) | $\Delta h_{r,2}$ J/mole |
|---|---|---|---|---|
| 1 | RWGS | $CO_2 + H_2 \leftrightarrows CO + H_2O$ | 1.61E9 | -108.0E3 |
| 2 | Hydrogenation | $CO + H_2 \leftrightarrows C(s) + H_2O$ | 1.49E7 | -42.3E3 |

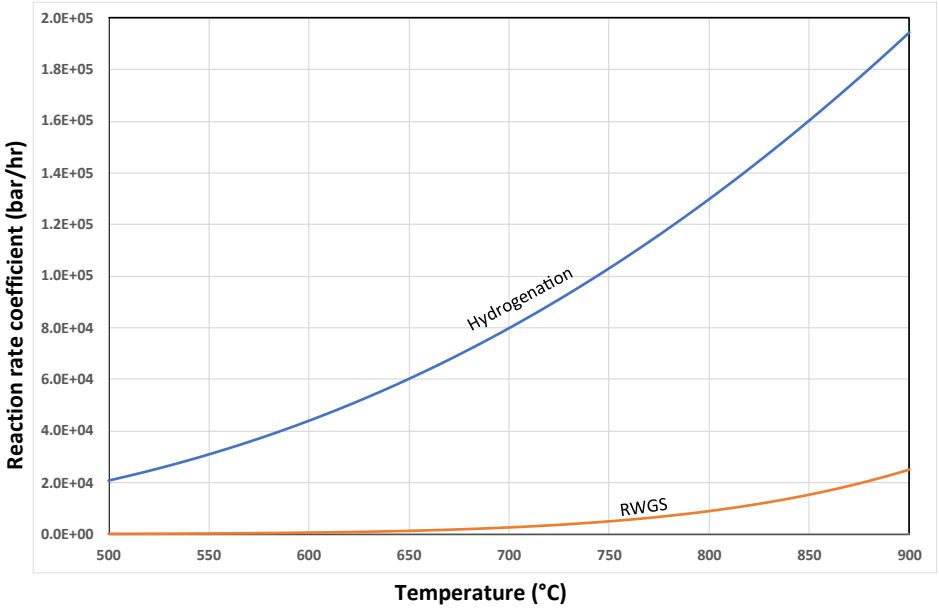


**Fig. 2. Reaction rates coefficients of RWGS, hydrogenation, and Boudouard reactions**

Table 2 lists the reference parameter values for the reaction rate and activation energy of the three reactions[5], equations 21, 22, and 23. Figure 2 shows these values within a 500-900 °C temperature range.

For the Boudouard reaction rate function, the model uses an approach proposed by Snoeck[6] that modeled the Boudouard reaction rate in the presence of the nickel carbide. The kinetics expression of Reaction 3 (Boudouard reaction) is stated as follows:

$$r_3 = \frac{\rho_c \varepsilon_p I_1 \tau_3 \left( P x_{co} - \frac{1}{\tau_4} \frac{x_{CO_2}}{x_{CO}} \right)}{1 + I_1 P x_{co} + \frac{1}{I_1 I_2} \frac{x_{CO_2}}{x_{CO}}} \quad (22)$$

$$\tau_3 = \tau_{r,3} exp\left(\frac{\Delta h_{r,3}}{R_g T}\right) \quad (23)$$

$$\tau_4 = \tau_{r,4} exp\left(\frac{\Delta h_{r,4}}{R_g T}\right) \quad (24)$$

Where
$r_3$ Boudouard reaction rate (mol/m$^3$-hr)
$\rho_c$ Carbon steel density (7,850 kg/m$^3$)
$\varepsilon_0$ Initial volumetric void fraction (-)
$\tau_3$ Primary Boudouard reaction rate coefficient (bar/hour)
$\tau_4$ Secondary Boudouard reaction rate coefficient (bar$^{-1}$)
$I_1$ The intermediate step of the reaction mechanism (0.113 bar$^{-1}$)
$I_2$ The intermediate step of the reaction mechanism (41.3 bar)
$x_i$ Mole fraction of component i (-)
$\tau_{r,3}$ Primary reference Boudouard reaction rate coefficient (bar/hour)
$\tau_{r,4}$ Secondary reference Boudouard reaction rate coefficient (bar$^{-1}$)
$\Delta h_{r,3}$ Primary reference Boudouard activation energy (Joule/mole)
$\Delta h_{r,4}$ Secondary reference Boudouard activation energy (Joule/mole)

***10) Catalyst degradation due to solid-graphite deposition:*** The deposition of solid carbon on the catalysis surface affects not only the volumetric void and the permeability of the porous packed bed of the reactor as estimated above, but also the efficiency of the catalysis degrading its performance. A preliminary and simple approach assumes that the degradation is linear and proportional to the volumetric void reduction. The reaction rate coefficients for all three S-Bosch reactions (RWGS, hydrogenation and Boudouard) expressed in Equations 20, 21, and 22, respectively, need to be corrected by a factor directly proportional to the reactor volumetric void, as illustrated below.

$$\tau_1{}' = \left[\frac{\varepsilon_p}{\varepsilon_o}\right] \tau_1 \quad (25)$$

$$\tau_2{}' = \left[\frac{\varepsilon_p}{\varepsilon_o}\right] \tau_2 \quad (26)$$

$$\tau_3{}' = \left[\frac{\varepsilon_p}{\varepsilon_o}\right] \tau_3 \quad (27)$$

Where
$\tau_1{}'$ Corrected WGS reaction rate coefficient
$\tau_2{}'$ Corrected hydrogenation reaction rate coefficient
$\tau_3{}'$ Corrected Boudouard reaction rate coefficient
$\varepsilon_o$ Initial/Starting volumetric void fraction.

**B. Geometry and scale**

The mathematical approach described above applies to 1D, 2D, and 3D domains. For the case presented in this paper, model geometry is a replica at a 1:1 scale of the actual tubular reactor built in-house at MSFC to perform the kinetics study. The tubular reactor is rotationally symmetric, and it is possible to reduce the model from a 3D to a 2D axisymmetric problem, as shown in Figures 3a and 3b, allowing us to model only half of the tube cross-section by assigning the center line of the reactor as a symmetry boundary. The catalysis is packed in the center of the tubular reactor, forming a porous section within the catalysis bed and two free-flow sections above and below the catalysis-packed bed, leading to two different gas flow regimes, as shown in Figure 3c.

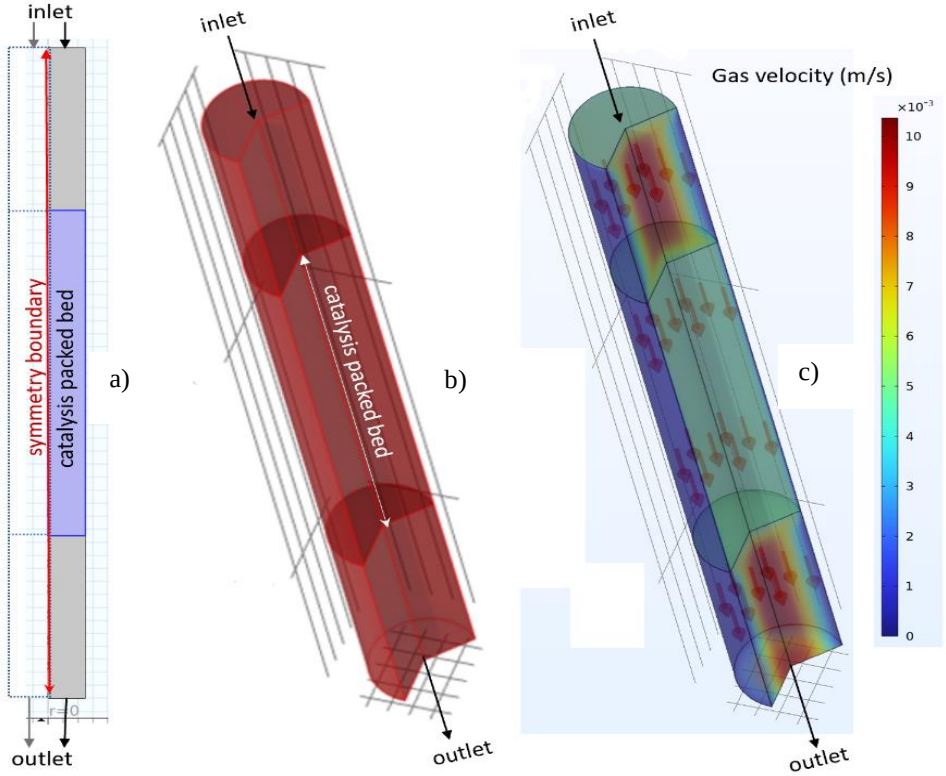


**Fig. 3. S-Bosch tubular reactor domain. a) Original 2D reactor domain, b) 3D reactor domain after 360-degree rotation of the 2D domain (a) around symmetry boundary, c) Modeled velocity profile throughout the 3D domain (b).**

### C. Boundary conditions

The relevant boundary conditions (BC) in the model include:

- Laminar Flow interface
  A normal inflow velocity drives the flow in the reactor at the inlet. The walls are represented by no-slip boundary conditions with a gas velocity equal to zero value.
- Transport of Concentrated Species interface
  At the inlet, the mass fraction of species is set to the experimental values. The outlet boundary condition is a convective flux condition. The convective flux condition implies that the species' diffusive flux is zero perpendicular to the boundary, which is a common assumption when modeling the outlet in tubular reactors.
- No-flux conditions.
  The no-flux conditions, called insulation/symmetry in COMSOL Multiphysics, are applied to all other boundaries. Across these boundaries, a no (total) mass flux condition is prescribed for all species.

### D. Mesh

A mapped (structured) mesh is used due to the tubular reactor's regular shape. The use of a structured mesh is especially suitable when the requirements for the mesh density are uneven. This case requires a denser mesh in the inlet region and the reactor wall, achieved by specifying the edge element distribution.

### E. Optimization algorithm

As stated above, an optimization algorithm can be used to perform 1) a kinetics study to determine the parameters of the reaction rate expressions for each reaction (WGS, hydrogenation, and Boudouard) and 2) Process optimization to determine the inlet conditions that lead to the highest conversion of $CO_2$ to solid carbon. For the kinetics study, the optimization algorithm aims to tune the parameters of the reaction rate expressions to minimize the accumulated error between the modeled and experimental values of selected output process variable values, such as the composition of the reaction products. For process optimization, the algorithm aims to tune the selected process condition variables, such as temperature, inlet flow rate, and inlet flow composition, to maximize the desired process outcome under a given set of process constraints, such as conversation, efficiency, and purity. It is recommended that the kinetics study be conducted first to determine the kinetics parameters and then optimize the process. The parameter values that lead

to local minima become candidates for the ultimate parameter values; additional optimization runs with different initial parameter values must be performed to be sure that the found local minima is the global minima.

Three optimization algorithms are available in COMSOL's optimization module for gradient-based optimization. The third algorithm is a Levenberg-Marquardt algorithm (LMA) solver. When using this solver, the objective function must be of least-squares type. Also, constraints are not supported. Since the Levenberg-Marquardt method is designed to solve problems of a least-squares type, it typically converges faster than the other two algorithms, Sparse Nonlinear OPTimizer (SNOPT) and Method of Moving Asymptotes (MMA), for such problems.

## III. Parametric Study

### A. Case Study

The tubular reactor has an inner diameter of 1 inch and a length of 4 inches filled with 2-mm diameter SS beads as catalyst packed in the middle of the tubular reactor, leaving 35% volumetric void in the packed bed section. Figure 4 illustrates the a) gas velocity that turns mostly uniform through the packed bed, b) the gauge pressure that, as expected, decreases through the packed bed, and c) volumetric void fraction that varies along the packed bed as solid carbon is generated by the hydrogenation and the Boudouard reactions (Equations 2 and 3) and deposited on the surface of the catalyst beads through the packed bed decreasing the void space of the reactor.

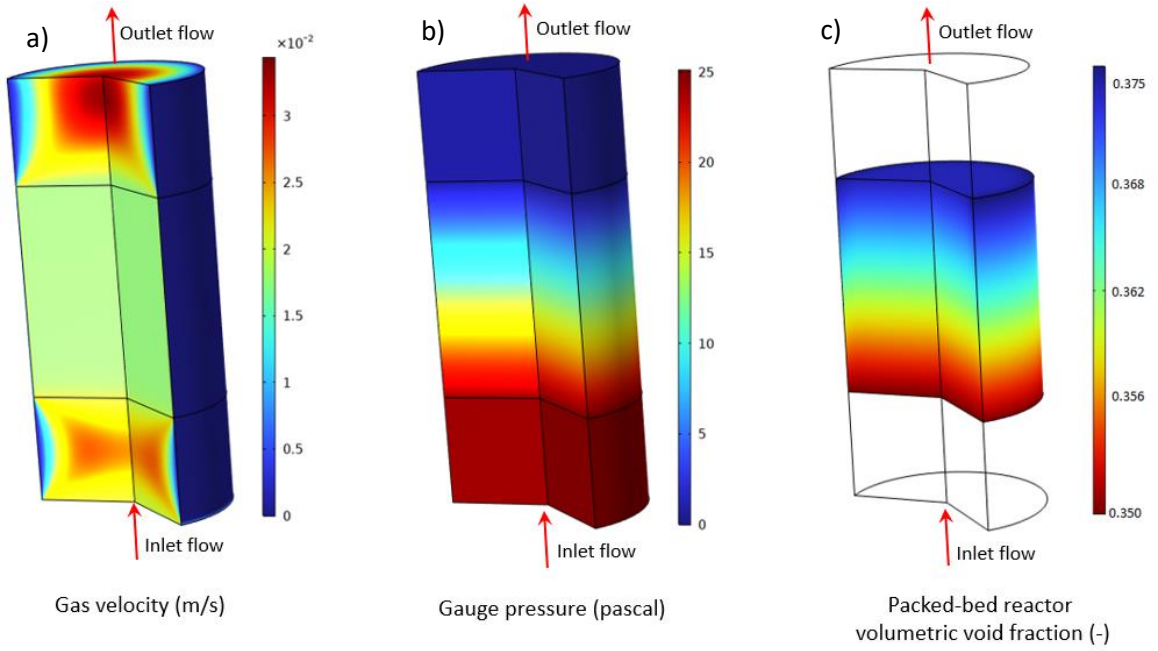


**Fig. 4. Model outcome profile of gas velocity, gauge pressure, and packed-bed reactor volumetric void fraction.**

Figures 5, 6, and 7 illustrate the model-based outcome of reaction rates, gas molar composition, and solid carbon deposition, respectively, as the reactor runs at 752 °C (1,025 K) temperature with an inlet binary $CO_2$-$H_2$ gas mixture of 20% $CO_2$ and inlet flow with a velocity of 0.002 m/s. It can be seen in Figure 5 that the hydrogenation and Boudouard reaction rates, which are those generating solid carbon, are within a comparable range through the packed bed, while the RWGS reaction rate is up to two orders of magnitude higher. The molar fraction of the species in Figure 6 shows that RWGS is the predominant kinetics, substantially reducing the $CO_2$ to CO and $H_2O$, and hydrogenation is the lesser, as a significant amount of CO is not reduced to solid carbon and water. The solid carbon generated by hydrogenation and Boudouard reactions shown in Figure 7 is assumed to be deposited on the surface of the catalyst beads altering the volumetric void fraction, and the Darcy permeability of the packed bed; Equations 13 and 14 are used to compute the variation of these two properties. The variation of the volumetric void faction on the packed bed is also used to compute the catalyst degradation due to solid-graphite deposition and its effect on the kinetics coefficient rates of all three S-Bosch reactions (Equations 25, 26, and 27, respectively).

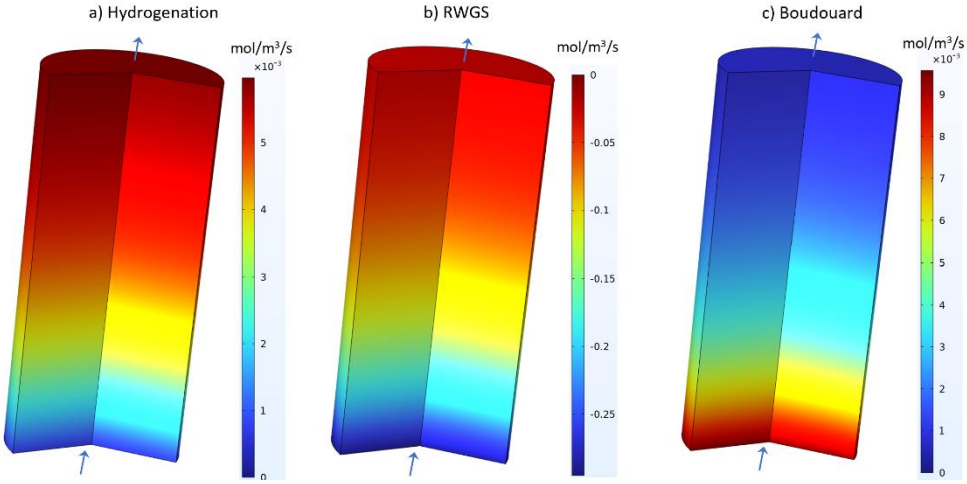


**Fig. 5. Reaction rates of the three coupled reactions, a) hydrogenation, b) RWGS, and c) Boudouard, throughout the packed bed of the reactor.**

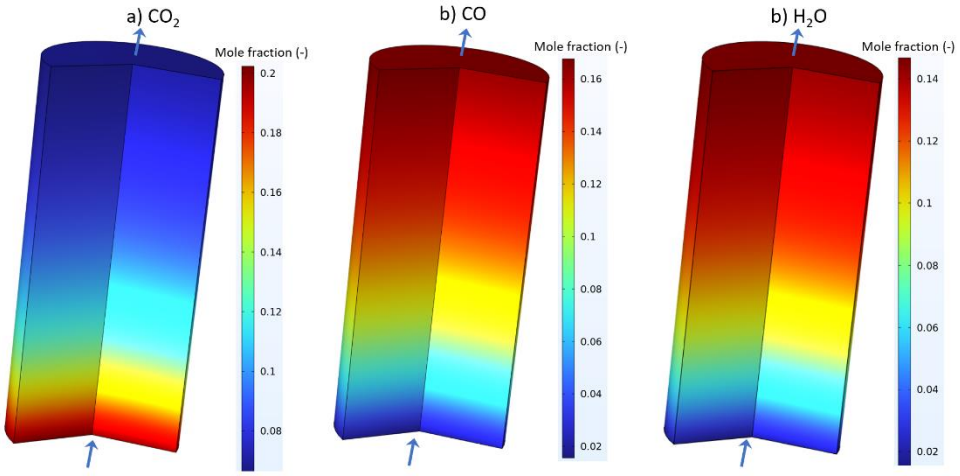


**Fig. 6. Molar fraction of a) $CO_2$, b) CO, and c) $H_2O$**

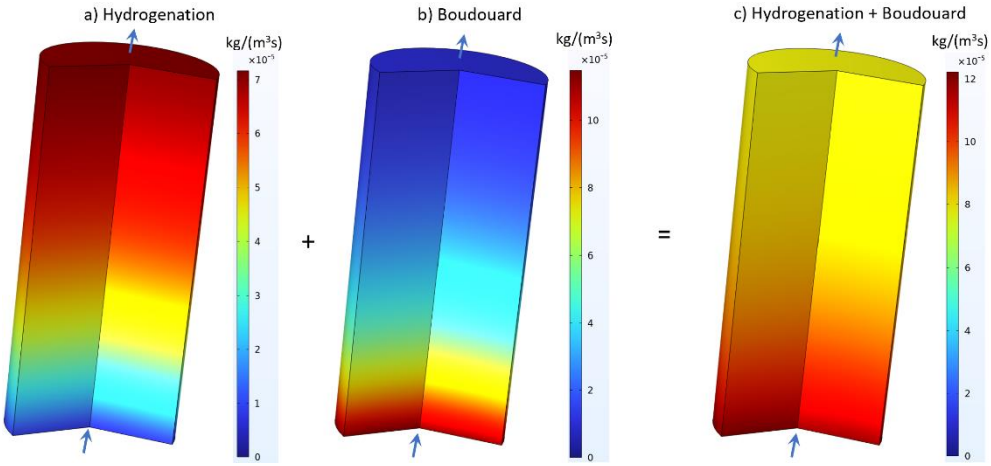


**Fig. 7. Solid carbon deposition from a) hydrogenation, b) Boudouard, and c) both**

## IV. Optimization

Taking the kinetic parameter values in Tables 1 and 2 for RWGS and the hydrogenation reactions and the kinetic parameter values published by Snoeck[6] for the Boudouard reaction, an optimization case using the LMA approach was conducted to find the temperature, inlet gas flow rate, and inlet $CO_2$-$H_2$ composition that achieve two optimization aims, maximum $CO_2$ recovery, and minimum CO composition. The optimization constraints rely on the input variables ranges, temperature: 577-977 °C (850-1,150 K), input $CO_2$ molar composition: 20-80%, and input flow rate: 0.002-0.02 m/s. LMA takes 982 iterations to find a global optimal 80.05% reduction of $CO_2$ at 1,150 K, 20% $CO_2$ molar percentage, and 0.006 m/s input flow rate. Figure 1 shows the $CO_2$ conversion (%) as a function of gas velocity and temperature at 20% $CO_2$ molar percentage.

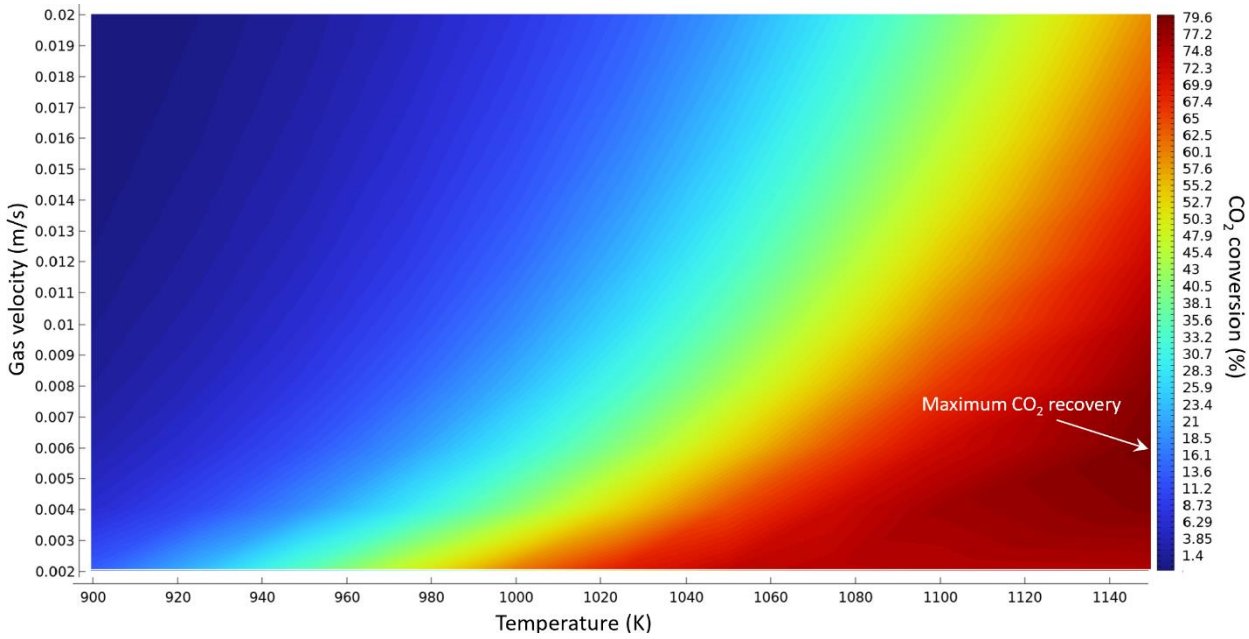


**Fig. 8. $CO_2$ conversion (%) as function of inlet gas velocity and temperature at constant $CO_2$ molar percentage (20%).**

Figure 9 shows the $CO_2$ conversion (%) as a function of temperature at constant inlet gas velocity (0.06 m/s) and $CO_2$ molar percentage (20%). As illustrated in Figure 9, the $CO_2$ reduction reaches an asymptotic value of 80% beyond 1,150 K.

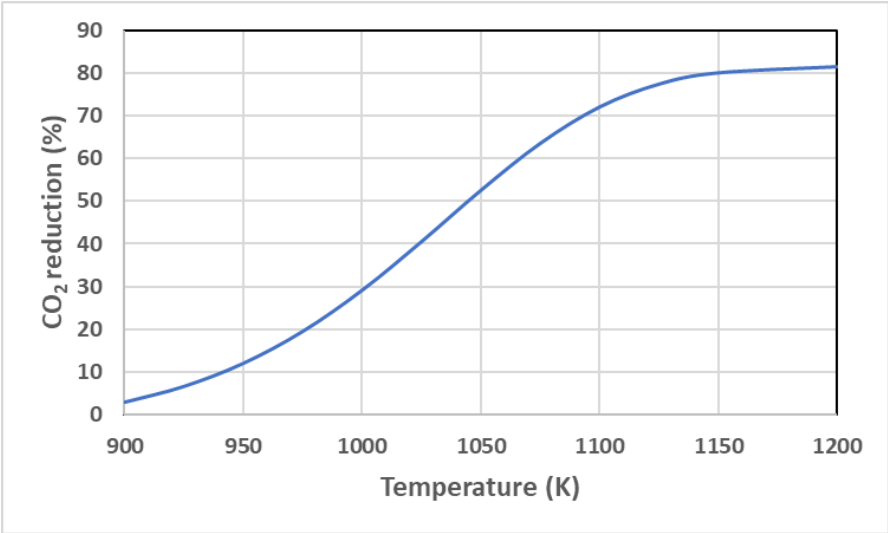


**Fig. 9. $CO_2$ conversion (%) as function of temperature at constant inlet gas velocity (0.06 m/s) and $CO_2$ molar percentage (20%).**

## V. Summary

The model is a unique dual tool that can be used to perform: 1) kinetics studies to characterize the catalysts by determining the respective temperature-dependent kinetics parameters of the three S-Bosch reaction rates and 2) process optimization to determine the input process conditions and reactor setup that maximize the $CO_2$ reduction and minimize energy consumption.

The model rigorously accounts for the fine solid carbon deposition on the surface of the catalyst and its effect on the volumetric void fraction, as well as the Darcy permeability of the packed-bed reactor. The hydrogenation and the Boudouard reactions simultaneously generate fine solid carbon by reducing $CO_2$ and CO, respectively, as stated in equations 2 and 3 of Figure 1. Since these two properties, Darcy permeability and void fraction, vary during the reactor's operation, the steady-state operation conditions are not reached, and the model must be implemented in the transient mode.

A primary outcome of the model is presented using equilibrium and kinetics rate parameters published by different researchers. they will be experimentally determined in-house via a kinetics study in the future to validate the S-Bosch reactor model, allowing the implementation of a parametric study and optimization of the S-Bosch process with a high degree of confidence.

## References

[1] Saurabh A. Vilekar, Kyle Hawley, Christian Junaedi, Dennis Walsh, Subir Roychoudhury, Morgan B. Abney, James M. Mansell, “Performance Evaluation of Staged Bosch Process for $CO_2$ Reduction to Produce Life Support Consumables,” 42nd International Conference on Environmental Systems, 15 July 2012 - 19 July 2012.
[2] Bunnell, C., Boyda, R., and Lee, M., “Otimization of the Bosch $CO_2$ reduction process," SAE International, 1991.
[3] Fritts, S., \Bosch Carbon Dioxide Reduction System Model," Tech. Rep. ESCG-4470-08-TEAN-DOC-0282, Engineering and Science Contract Group, Houston, TX, June 2008.
[4] Sandler, S., Chemical and engineering thermodynamics, John Wiley & Sons, 1989.
[5] Fritts, S., \Bosch Carbon Dioxide Reduction System Model," Tech. Rep. ESCG-4470-08-TEAN-DOC-0282, Engineering and Science Contract Group, Houston, TX, June 2008.
[6] Snoeck, J., Froment, G., and Fowles, M., \Steam/CO2 Reforming of Methane. Carbon Filament Formation by the Boudouard Reaction and Gasification by CO2, by H2, and by Steam: Kinetic Study," Industrial Engineering & Chemical Research, Vol. 41, 2002, pp. 4252-4265.